JOURNAL OF GEOPHYSICAL RESEARCH, VOL. 106, NO. D14, PAGES 15,029–15,044, JULY 27, 2001

Airborne studies of cloud structures over the Arctic Ocean and comparisons with retrievals from ship-based remote sensing measurements

Peter V. Hobbs and Arthur L. Rangno

Department of Atmospheric Sciences, University of Washington, Seattle

Matthew Shupe

Science and Technology Corporation, Hampton, Virginia

Taneil Uttal

NOAA Environmental Technology Laboratory, Boulder, Colorado

Abstract. Information on the heights and microphysical structures of two cloud systems derived from a 35 GHz radar, microwave and infrared radiometers, and a lidar aboard a ship in the Arctic Ocean are compared with simultaneous airborne in situ measurements. The cloud systems considered are a single layer of thin altocumulus with virga (June 3, 1998), and a more complex cloud system consisting of several altocumulus-altostratus layers that precipitated into a boundary layer, stratus-stratocumulus system (May 29, 1998). For the first cloud system the cloud top deduced from the 35 GHz radar was close to that measured from the aircraft. The radar detected virga below cloud base even when the virga was composed of very low concentrations of ice crystals; this prevented measurement of the cloud base height with the radar. Because of the sensitivity of the 35 GHz radar to ice crystals, cloud liquid water contents derived from it are confounded by just a few ice crystals. In the case of the second more complex cloud system, embedded cloud liquid water layers into which ice particles fell were not resolved by the radar. Consequently, although five altocumulus layers were intercepted by the aircraft, the radar display depicts a single deep precipitating system. These cases illustrate that liquid water content in mixed-phase clouds cannot be retrieved reliably using the radar-microwave radiometer technique.

1. Introduction

Clouds play an important role in the radiative balance of the Arctic. Therefore documentation of their occurrence and properties was an important part of the First ISCCP (International Satellite Cloud Climatology Project) Regional Experiment-Arctic Clouds Experiment/Surface Heat Budget in the Arctic (FIRE-ACE/SHEBA) field project in the Arctic in 1997-1998. A potentially valuable source of data in this respect was the almost continuous measurements of clouds provided by the National Oceanic and Atmospheric Administration (NOAA)/Environmental Technology Laboratory (ETL) 35 GHz radar, microwave, and infrared radiometers, and a lidar, all of which were aboard the Canadian Coast Guard ship *des Groseilliers* (hereinafter referred to as "the ship") as it drifted with the ice in the Arctic Ocean throughout the 1-year period of the SHEBA field study. Therefore it is crucial to evaluate the reliability of various cloud properties derived from the shipboard remote sensing systems. In this paper we make a start on this task by comparing some of the cloud and precipitation parameters derived from various remote sensing instruments aboard the ship with simultaneous in situ measurements obtained from the University of Washington Convair-580 research aircraft as it flew in the vicinity of and directly over the ship.

Two case studies are described. These are a slightly supercooled, thin altocumulus layer, and a more complex system of many interacting cloud layers. In both cases the location of the measurements was deep in the Arctic, at a latitude of about 77°N.

Paper number 2000JD900323.
0148-0227/01/2000JD900323$09.00

2. Observing Systems and Techniques

The 35 GHz radar [*Moran et al.*, 1998], and the methods used to retrieve cloud properties from this radar, are described by *Shupe et al.* [this issue]. In brief, the radar was an unattended system that pointed vertically and provided continuous radar echo profiles through clouds and light precipitation. The single polarization system used a low-peak-power, high-duty-cycle traveling wave tube amplifier transmitter, a high-gain antenna, and pulse compression techniques. The pulse compression techniques make the radar particularly sensitive, with estimated detection capabilities of -47 dBZ at 5 km. The range resolution was 45 m. In the Arctic environment, attenuation was rarely, if ever, an issue.

The microwave water radiometer (MWR) aboard the ship was a Radiometrics WVR-1100, which receives at 23.8 and 31.4

GHz. The MWR provides time series measurements of column-integrated water vapor and liquid water. The instrument was tuned to measure microwave emissions from vapor and liquid water molecules at specific frequencies.

Liquid water content retrievals, given in this paper, are based on information on integrated liquid water path from the microwave radiometer and profiles of reflectivity from the 35 GHz radar. This technique has been discussed by *Frisch et al.* [1998]. Certain modifications, based on relationships between droplet concentrations and calculated radar reflectivities (A. S. Frisch et al., On the retrieval of effective radius with cloud radars, manuscript in preparation, 2001), were applied to the present data sets. The technique can be applied to multiple liquid layer clouds and liquid clouds distinctly separated from ice clouds that may exist in the same atmospheric column. However, as will be demonstrated in this paper, this technique cannot be applied to mixed-phase clouds or other precipitating clouds. This is because even low concentrations of ice crystals can dominate the radar reflectivities and render liquid water retrievals erroneous. The same is likely to be true of clouds containing drizzle drops.

Also aboard the ship was an Atmospheric Emitted Radiance Interferometer (AERI), which measured the absolute infrared spectral radiance of the sky directly above the instrument. The spectral measurement range of the instrument was 500 to 3300 cm^{-1} (or 20 to 3 μm), the spectral resolution 1.0 cm^{-1}, and the field of view 1.3°. A calibrated sky radiance spectrum was produced every 10 min from which an IR sky brightness temperature was calculated. This brightness temperature was used to determine the optical depth of ice clouds.

Ice retrievals incorporated the estimates of optical depth from the AERI to develop tuned values for the "*a*" coefficient for an ice water content (IWC)-reflectivity(Z) relationship of the form suggested by *Matrosov* [1999]:

$$\mathrm{IWC} = aZ^b \tag{1}$$

The "*b*" coefficient in equation (1) takes an assumed profile shape according to *Matrosov* [1999]. In the cases where the optical depth is too thin to provide reasonable estimates of the "*a*" coefficient, or the presence of liquid water in the atmospheric column contaminates the infrared measurements, it is necessary to assume a value of "*a*." In these cases "*a*" can be subjectively chosen on the basis of observations of clouds with similar reflectivity and altitude characteristics, or it can be set to the mean value of "*a*" calculated for the SHEBA/FIRE-ACE time period. In general, this method of tuning equation (1), whether through direct use of IR measurements or by applying a subjective coefficient, is expected to be considerably more accurate than the many generic IWC-Z relationships, which produce IWC values ranging over orders of magnitude [*Matrosov,* 1997].

Ice particle characteristic size is calculated from the IWC using the relationship

$$Z = GD_0^3(\mathrm{IWC}), \tag{2}$$

where D_0 is the equivalent volume median diameter of the ice particle, and the coefficient G is a function of the particle shape, density, and size distribution type [*Atlas et. al.*, 1995]. Mean particle diameter can be calculated from D_0 using a conversion factor that assumes an exponential particle size distribution.

The NOAA/ETL depolarization and backscatter lidar provided information on the phase (water or ice) of clouds [*Alvarez et al.,* 1998]. This is a pulsed laser-radar system operating at 523 nm wavelength. The lidar range resolution is 30 m with real-time averaging of 5 s applied to reduce the data load and provide a sufficient signal-to-noise ratio for observing clouds and aerosols. The system produces two main fields of information: returned power (which depends on the density of the scatterers) and the depolarization ratio (which gives an indication of the shape, and hence phase, of the scatterers). Lidar measurements were not specifically employed in the microphysical retrievals but were instead used to subjectively determine the phase of certain cloud layers.

The instruments aboard the Convair-580 for in situ cloud microstructural measurements were the same as those described by *Hobbs and Rangno* [1998] but with the addition of the recently available SPEC Inc. Cloud Particle Imager (CPI) [*Lawson and Jensen,* 1998]. The CPI can record up to 30 cloud particle images per second and resolves particles down to about 15 μm in maximum dimensions (MDs). It can also record the size spectrum and concentrations of particles from ~5 to 2500 μm MD. Particle concentrations were also measured with a Particle Measuring System (PMS) two-dimensional (2-D) cloud probe [e.g., *Heymsfield and Parrish,* 1978]. These latter concentrations are conservative estimates because they do not include particles <100 MD. Cloud liquid water contents (LWC) were measured with a PMS Forward Scattering Spectrometer Probe (FSSP-100) [e.g., *Dye and Baumgardner,* 1984] and the Gerber Scientific Particle Volume Monitor-100 (PVM-100) [*Gerber et al.,* 1994]. The LWC from the FSSP-100 and PVM-100 were in excellent agreement. However, in this paper the measurements of LWC are from the PVM-100.

3. June 3, 1998, Case: A Single Layer of Thin Altocumulus With Virga

On June 3, 1998, a weak high-pressure ridge extended from the eastern Beaufort Sea to the ship (Figure 1). The winds over the ship were light and from the southeast from the surface to above 400 hPa. Relatively thin altocumulus clouds showing virga were over the ship (virga is precipitation that does not reach the ground). The ship itself was occasionally immersed in "ground fog," which topped out at about the height of the ship's stack.

3.1. Radar and Lidar Observations

During the University of Washington (UW) Convair-580 flight over the ship on June 3, the 35 GHz radar (Plate 1) indicated a layer of enhanced reflectivities (–20 dBZ to –5 dBZ) from just below 2 km to about 3 km (all heights are above mean sea level) and a curtain of lower reflectivities (<–20 dBZ) below 2 km up to 2200 UTC. After 2200 UTC the radar returns below 2 km disappeared for the most part, with the exception of a near-surface return below 1 km between 2230 and 2330 UTC. Between 1400 and 2000 UTC (only the period 2000-2200 UTC is shown in Plate 1) there was a radar bright band at 0.5 km caused by a layer of melting ice particles; this layer seemed to be associated with the lowest liquid layer detected by the lidar.

Ship-based measurements from the depolarization lidar suggested that the top of the altocumulus layer was liquid water during the period of the Convair-580 flight over the ship there

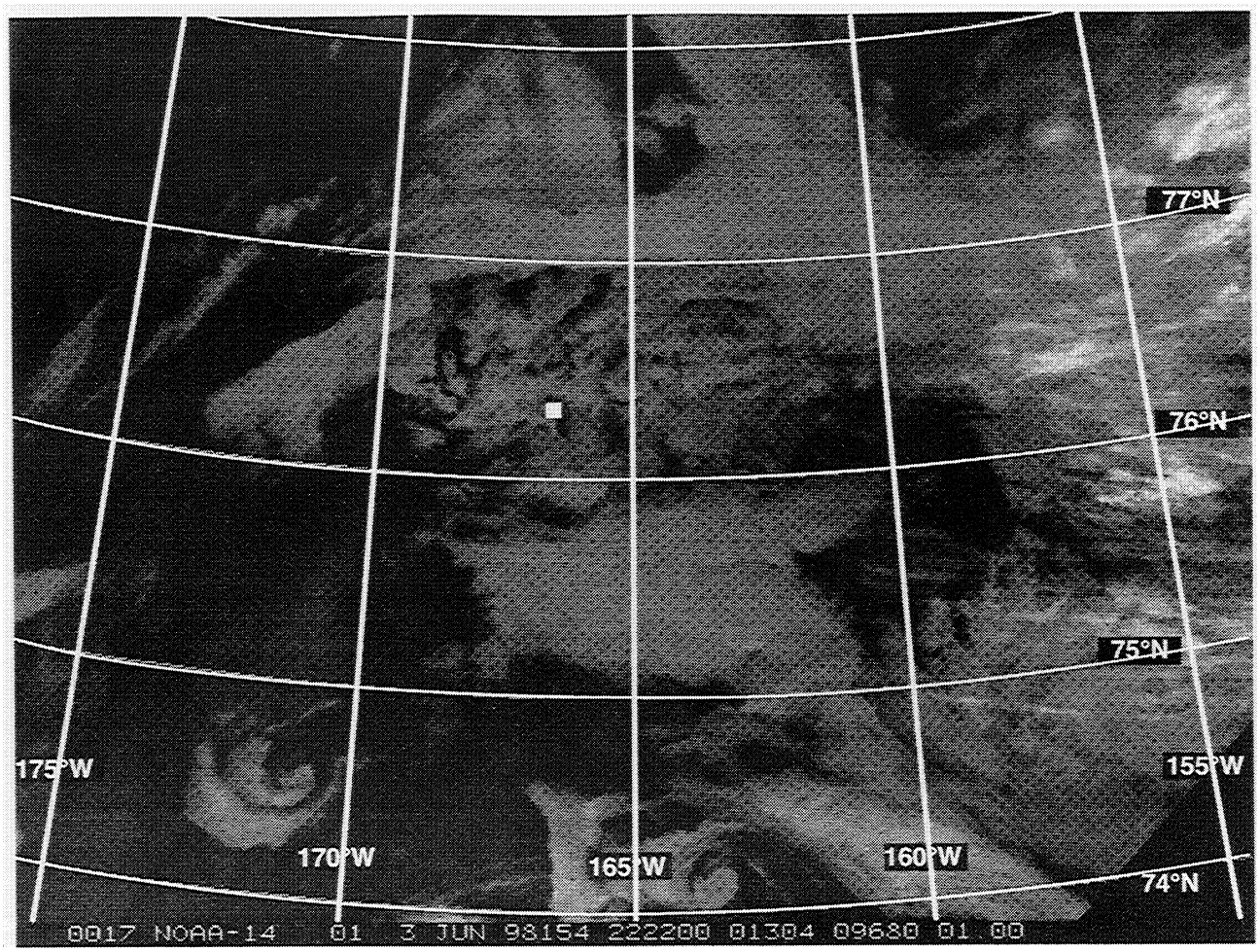

Figure 1. Infrared satellite image at 2222 UTC, June 3, 1998, during the time that measurements were obtained from the UW Convair-580 aircraft over the SHEBA ship (white square).

were smaller amounts of liquid mixed with ice between about 2.25 and 2.75 km. The lidar also observed a second layer of liquid between about 0.6 and 0.75 km, below which was liquid and mixed-phase precipitation.

3.2. Airborne in Situ Measurements and Comparisons With Retrievals From Remote Sensing Instruments on the Ship

Table 1 and Figure 2 provide details on the altocumulus perlucidus cloud layer and the virga it produced from the perspective of the in situ measurements made from the aircraft. The cloud was well mixed with a pseudoadiabatic lapse rate.

The altocumulus layer was sampled twice from the aircraft: the first time between 2121:49 and 2122:47 UTC when cloud top and cloud base were intercepted at 2.96 and 2.65 km and then more extensively between 2214 and 2239 UTC with cloud top and cloud base at 3.10 and 2.75 km. These measurements were obtained within 40 km from the ship in a fairly uniform cloud. In fact, there was little change in the composition of the cloud between these two time periods (Table 1). Also, in both cases, low concentrations of stellar and dendritic ice crystals (<1 per liter) precipitated from the layer (Figure 3). Some of these crystals survived to 2.00 km (−7°C), i.e., to about 700 m below the liquid water base of the altocumulus layer. The amount of virga from the altocumulus layer was visually noticeably greater during the ascent of the aircraft, when there were several scattered areas where the virga was so heavy that the background behind the virga could not be seen. The average droplet concentrations in the two penetrations of the cloud layer were 90 and 55 cm^{-3}, respectively. The LWC averaged 0.10 and 0.05 g m^{-3}, respectively. The average effective cloud droplet radius of the two samples were 8.1 and 7.7 μm, respectively.

A casual inspection of the radar reflectivity shown in Plate 1 would suggest that after about 2200 UTC the base of the altocumulus cloud layer was just below 2 km. In fact, as we have just described, the aircraft measurements showed the base to be at 2.75 km. The reason for the apparent discrepancy in heights is that 35 GHz radars are very sensitive to low concentrations of ice particles [*Hobbs et al.*, 1985], and therefore the radar detected the ice particles below cloud base even though they were very few in number.

The airborne measurements obtained in the descent showed the LWC in the altocumulus layer decreasing almost linearly with decreasing height (Figure 4a). During the subsequent ascent of the aircraft over the ship, the altocumulus layer was sampled more extensively and the LWC profile hints at the presence of two layers (Figure 4b). Figure 4a shows LWC in the altocumulus layer retrieved from the shipboard radiometer and radar reflectivity measurements. These retrievals show

Table 1. Summary of the Microstructural Properties of the Clouds Over the SHEBA Ship on June 3, 1998, Derived From in Situ Measurements Aboard the UW Convair-580 Research Aircraft

Time of Intercept (hhmm:ss, UTC)	Type of Cloud	Cloud Top Height (km)	Cloud Top Temperature (°C)	Cloud Base Height (km)	Cloud Base Temperature (°C)	Cloud Depth (m)	Average Droplet Concentration (cm^{-3})	Average Liquid Water Content (g m^{-3})	Maximum Liquid Water Content (g m^{-3})	Average Tail of the Droplet Spectrum (μm)	Maximum Tail of the Droplet Spectrum (μm)	Average Effective Radius of Cloud Droplets (μm)	Average Concentration of Drizzle Drops (per liter)	Maximum 1 km Drizzle Drop Concentration (per liter)	Liquid Water Path (g m^{-2})*	Average Ice Particle Concentration (per liter)	Maximum 1 km Ice Particle Concentration (per liter)	Types of Ice Particles
2146:43-2151:01	ground fog	0.028	-0.5	0.00	0*	30	40	0.02	0.05	17	23	7.3	0	0	0.6	0.00	0.00	none
2128:40-2128:50	stratus	0.75	-0.9	0.68	-0.5	70	65	0.03	0.07	13	18	5.5	0	0	2.1	0.00	0.00	none
2129:13-2129:30	stratus	0.56	0.5	0.47	0.2	90	70	0.06	0.1	20	22	7.7	0	0	5.4	0.00	0.00	none
2121:49-2122:47	alto-cumulus	2.96	-14.9	2.65	-12.6	310	90	0.1	0.21	19	23	8.1	0	0	31	0.18	0.32	stellars, dendrites, irregulars
2214:24-2239:03	alto-cumulus	3.10	-15.1	2.75	-12.9	350	55	0.05	0.17	18	29	7.7	0	0	18	0.35	1.75	stellars, dendrites, irregulars

*Estimate.

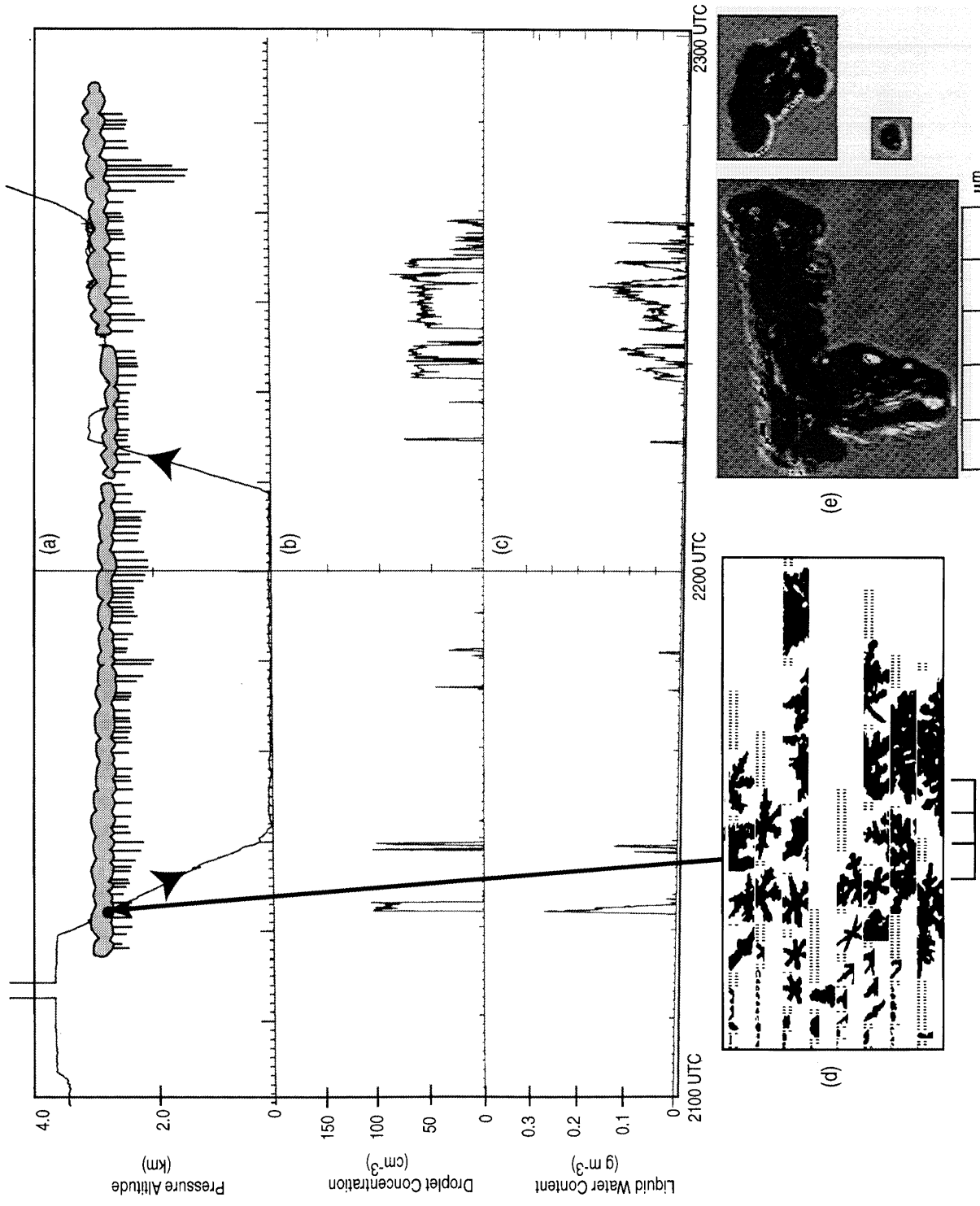

Figure 2. Overview of the clouds sampled by the UW Convair-580 aircraft between 2100 and 2300 UTC on June 3, 1998. (a) Schematic of clouds intercepted. The aircraft track is shown by the line with the arrows on it. (b) In situ measurements of droplet concentrations from aircraft. (c) In situ airborne measurements of liquid water content from the FSSP-100 (solid line) and the PVM-100 (dashed line); the measurements from these two instruments are essentially identical. (d) Examples of ice particles imaged by the PMS 2-D cloud probe from 2122:19-2123:29 UTC. (e) Examples of ice particles imaged by the CPI in the same cloud region as Figure 2d.

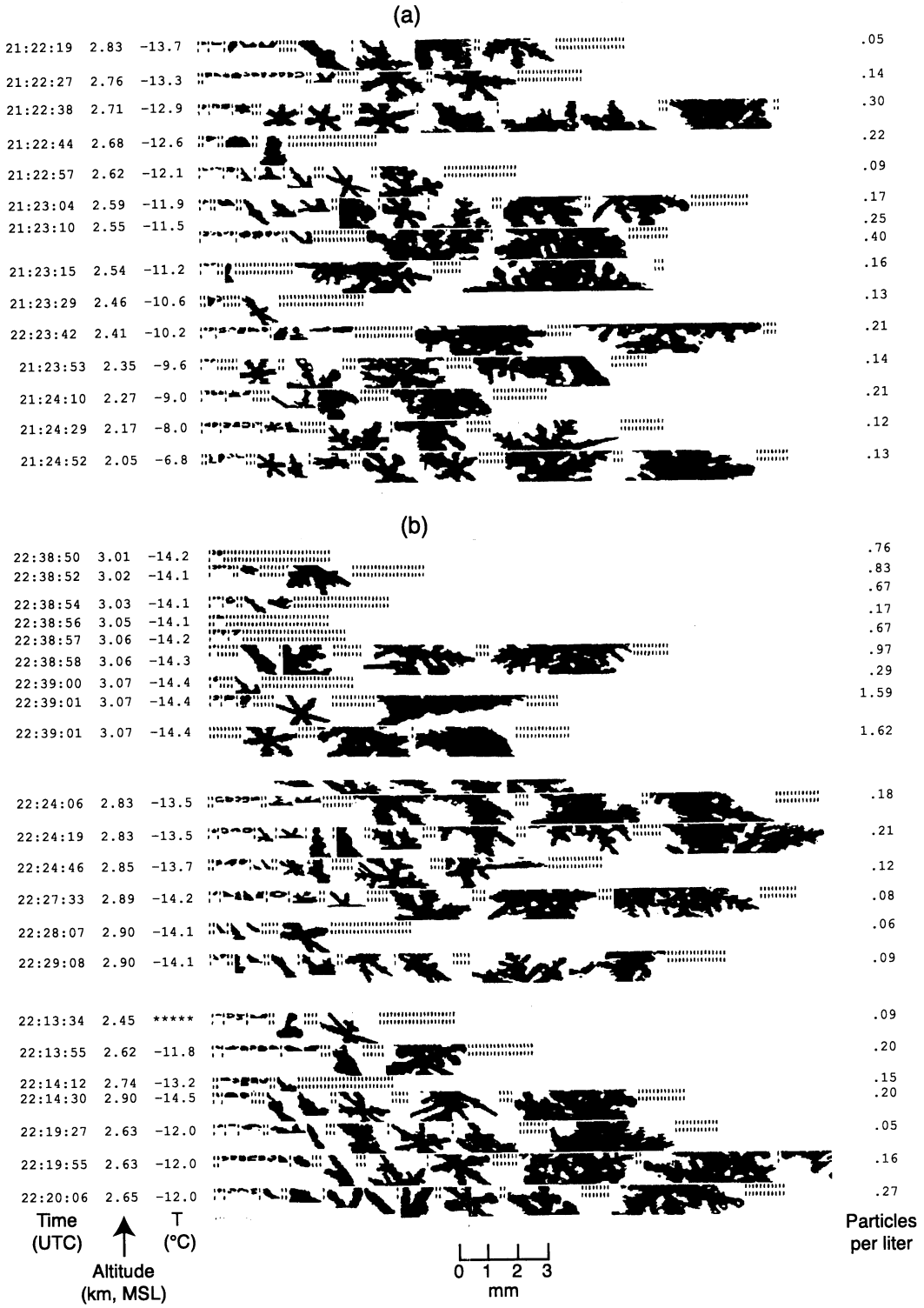

Figure 3. (a) Images of ice particles from the PMS 2-D cloud probe obtained in and below an altocumulus cloud layer (Figure 3a) during the descent of the UW Convair-580 aircraft over the SHEBA ship, and (b) during the aircraft's ascent over the SHEBA ship on June 3, 1998. The small vertical tick marks denote the beginning and ending of size bins 100 μm in width.

exactly the reverse trend with height to the in situ airborne measurements. The reason for this is that ice crystal concentrations in the cloud increased toward cloud base and, because of the sensitivity of the radar to low concentrations of ice particles, the reflectivity from the ice dominated that from the liquid water. This illustrates very clearly that liquid water in mixed-phase clouds cannot be retrieved using the microwave-radar technique.

Single ice crystals were the rule, both within and below the altocumulus layer; aggregates comprised no more than 5% of all the ice particles encountered. Most of the ice particles showed little or no riming, which is compatible with the fairly

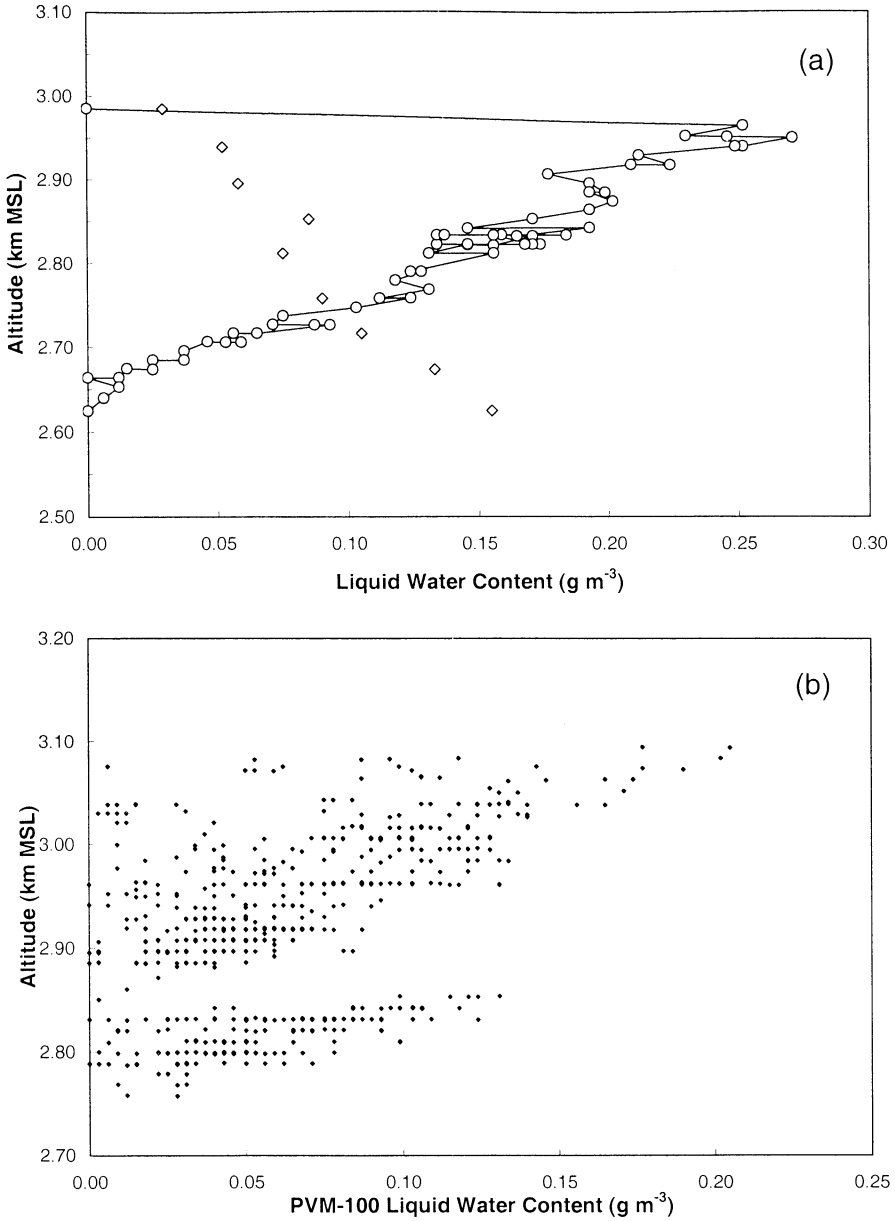

Figure 4. (a) Circles connected by the line are cloud liquid water content (LWC) from the PVM-100 in the altocumulus layer measured from the UW Convair-580 aircraft during its descent over the SHEBA ship on June 3, 1998. The diamonds are the LWC retrieved from the shipboard radiometer and radar reflectivity measurements. (b) Vertical profile of LWC measured from this aircraft during the more extensive measurements obtained in its ascent over the SHEBA ship.

small droplets in the cloud and the fact that many of the crystals did not reach sizes where riming occurs (i.e., >300 μm MD). For example, the average tail of the droplet spectrum, which provides a measure of the largest cloud droplets present, was at only 19 and 18 μm diameter, respectively, in the two penetrations of the cloud layer. The maximum droplet tail values near the top of the cloud layer were 22 μm during the descent and 29 μm on the ascent.

In the vicinity of the ship (but not exactly over it) a few wisps of two scattered stratus clouds were intercepted by the aircraft for a few seconds near the surface (at 0.7 and 0.5 km, respectively), as was the top of a ground fog at about 30 m above the surface (Table 1). These clouds also had quite low droplet concentrations (30-70 cm^{-3}), but they were too shallow to produce large drops or drizzle. The aircraft measurements indicated that the altocumulus layer was only 300-350 m thick (Table 1 and Figure 2), with a 700 m thick fallout region below cloud base that was composed of a few stellar-type ice crystals and their agglomerates (concentrations <1 per liter).

Because the altocumulus layer on June 3 was mixed phase, it was not suitable for the retrieval of some cloud properties, particularly liquid parameters, using the radar-radiometer technique (as demonstrated by Figure 4). However, it was the type of cloud that predominated during spring and summer over the SHEBA ship [*Shupe et al.*, this issue]. Since radar reflectivity is related to the sixth power of the particle size, the large particles in this mixed layer dominated the radar

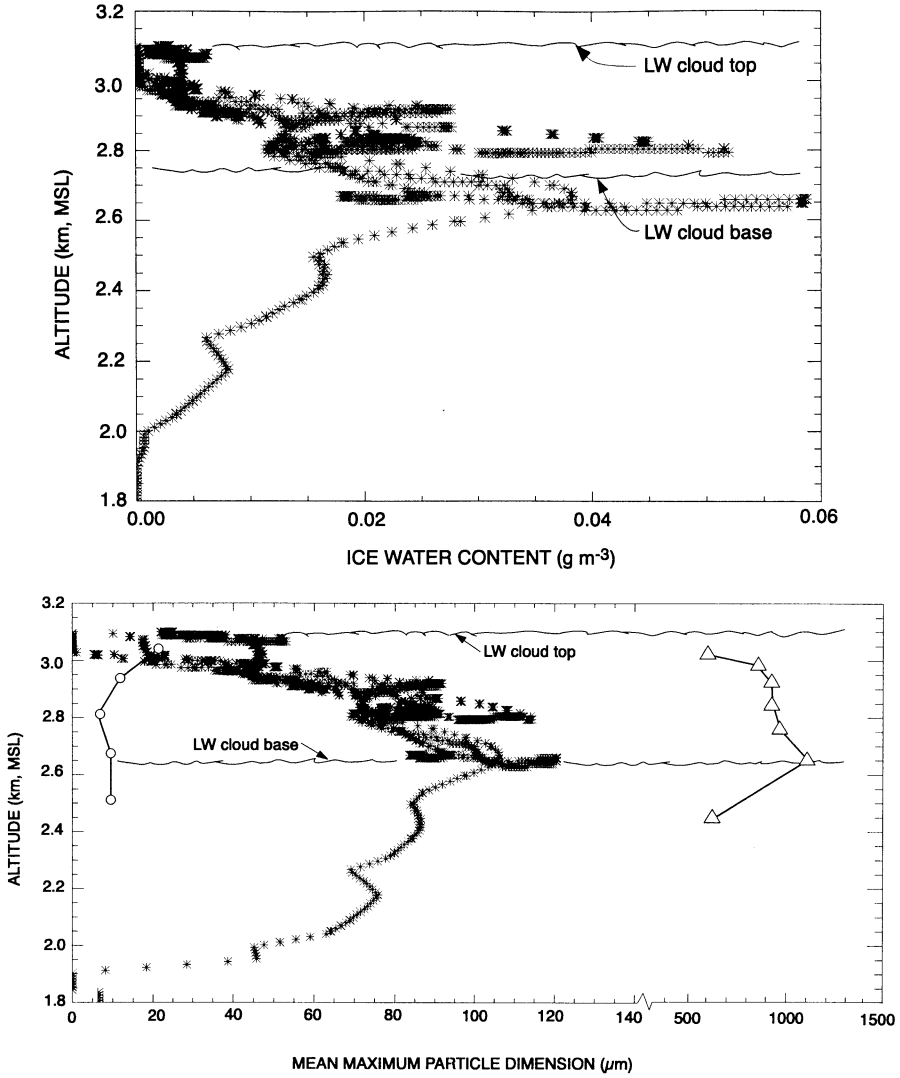

Figure 5. (a) Ice water contents (IWC) retrieved from ship-based remote sensing measurements using equation (1) for the period when the aircraft was ascending over the ship. The scalloping denotes the locations of the base and top of the altocumulus layer measured from the aircraft. (b) As for (Figure 5a) but for retrieved (asterisks) measurements of mean particle diameter derived from equation (2) and airborne in situ measurements of mean maximum dimensions of ice particles with MD ≥100 μm from PMS 2-D cloud probe (triangles) and particles with MD from 5 μm to 2.5 mm from the CPI (circles). The PMS and CPI measurements are dominated by ice particles and cloud droplets, respectively.

signal on June 3. Therefore radar-based retrievals of ice water contents and crystal size were calculated through the depth of the cloud using equations (1) and (2), respectively. It is assumed that these retrieved profiles are representative of the ice crystals embedded in the cloud. Since the IR measurements were dominated by the liquid in the cloud, the "*a*" coefficient in equation (1) was chosen on the basis of the mean value of this coefficient observed during the SHEBA/FIRE-ACE time period.

The retrievals of IWC are shown in Figure 5a. They are qualitatively consistent with the airborne in situ measurements in showing the amount of ice to be greatest near the base of the altocumulus layer and decreasing rapidly with increasing height above cloud base. Figure 5b shows retrieved ice particle mean diameters. Also shown in Figure 5b are the mean MD of the particles from the airborne measurements with the CPI and the PMS 2-D cloud probe. The large difference in the measured mean maximum dimensions between the CPI and the PMS 2-D cloud probe is due to the sizes of the particles each probe is able to measure. The CPI images cloud droplets as small as 10-20 μm in diameter quite effectively. Therefore in mixed-phase clouds the CPI is dominated by images of cloud droplets, since they generally exist in concentrations several orders of magnitude greater than the ice particles. Thus the CPI measurements shown in Figure 5b represent primarily the liquid drops in the altocumulus cloud. On the other hand, because the sizes of even the largest drops in this cloud were less than 25 μm diameter, which is below the detection limit of the PMS 2-D cloud probe, the PMS 2-D measurements represent the maximum diameters of the ice particles in the cloud. The ice particles were several times larger than the largest drops.

In general, the mean particle size profile retrieved from the radar has a similar shape to that measured by the PMS probe. However, there are differences in the absolute sizes. This could be due, in part, to an assumed one-to-one aspect ratio in

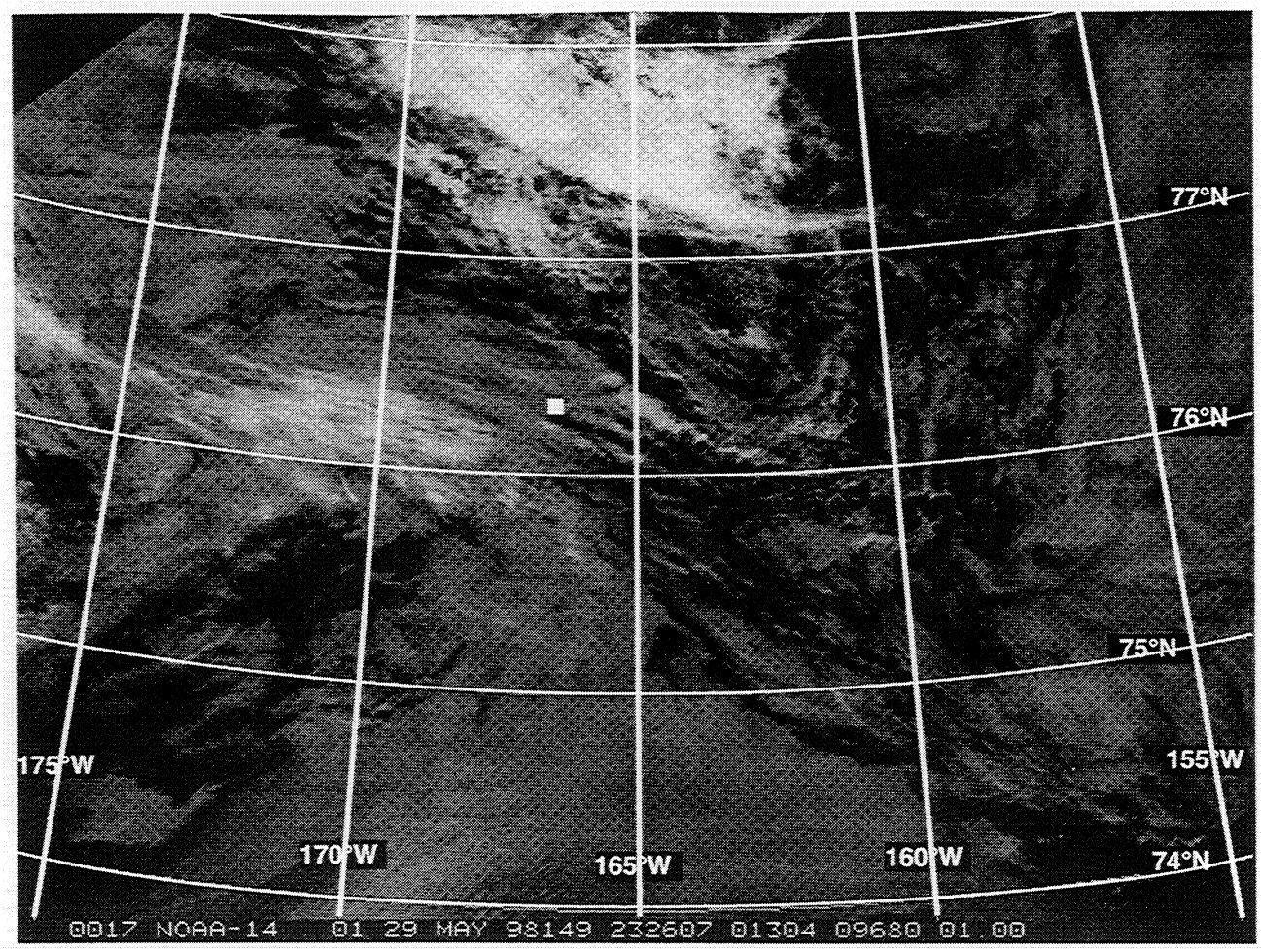

Figure 6. Same as Figure 1 but at 2326 UTC, May 29, 1998, or about 1 hour after the UW Convair-580 aircraft began its ascent over the SHEBA ship (white square).

the radar retrieval of ice particle size, which is not always the case (see Figures 1 and 2).

4. May 29, 1998, Case Study: Complex Multiple Cloud Layers

On May 29, 1998, a small low-pressure center (1007 hPa) located just north of the ship was moving northeastward away from the ship. At 500 hPa a weak trough extended from virtually overhead of the ship southwestward toward Siberia. The flow aloft was very light (<5 m s^{-1}) and generally southerly. The satellite imagery shows a very chaotic, multilayered cloud situation during the time of the UW Convair-580 measurements over the ship (Figure 6).

4.1. Deductions From Ship-Based Remote Sensing Measurements

The echo return from the shipboard vertically pointing 35 GHz radar between 1200 UTC, May 29, and 0000 UTC, May 30, shows a deep cloud system with tops to about 5.5 km. Rain was reported at the ship at 1200 and 1800 UTC, May 29. There was a persistent radar bright band at about 1.2 km. Beneath the bright band, radar Doppler velocities in excess of 1.5 m s^{-1} clearly indicated that drizzle and/or light rain was occurring. Because the lidar was completely attenuated by the drizzle and rain, the surface sensors can provide no direct observation of whether the cloud above the bright band was all ice, or mixed ice and liquid. The measurements from the AERI were also saturated by the liquid in the precipitation; therefore it was not possible to do the type of radar-IR radiometer retrieval described by *Matrosov* [1999]. However, the radar-IR radiometer retrieval was run for May 27, when an all-ice cloud was present which had somewhat similar radar reflectivities, thickness, and altitude characteristics to that on May 29. The May 27 retrieval provided the "*a*" coefficient used in equation (1) for calculating the IWC on May 29. Even if the cloud above the bright band was a mixture of liquid and ice, the radar reflectivities would be dominated by the large ice crystals, so contributions from the liquid drops would not significantly impact the IWC estimates. The results of the IWC and LWC retrievals are shown in Plate 2. The derived IWC ranged from 2 $\times 10^{-5}$ to 9.0 $\times 10^{-2}$ g m^{-3}. Below the bright band, the radar echo was completely dominated by rain and/or drizzle.

At 2240 UTC the cloud that had relatively stable characteristics for the preceding 31 hours began to dissipate, and by 2315 UTC, it had broken up into a two-level system.

4.2. Airborne Measurements and Comparisons With Ship-Based Observations

The back edge of the cloud system was approaching the ship as the Convair-580 neared the ship. Consequently, there was a considerable change in the vertical cloud layering between the

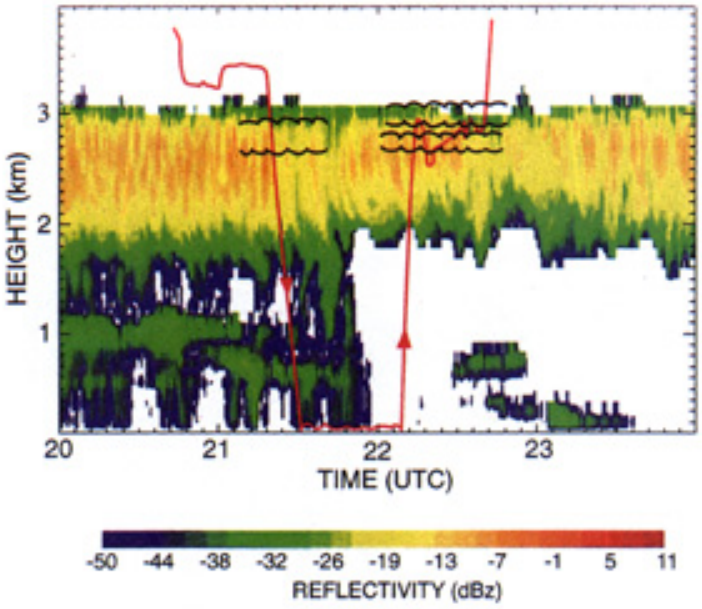

Plate 1. The 35 GHz radar reflectivity returns from the ice-shedding altocumulus layer from 2000 UTC, June 3, to 0000 UTC, June 4, 1998. Line with arrow shows the UW Convair-580 aircraft flight path. Scalloping denotes the bases and tops of the droplet clouds measured from the aircraft.

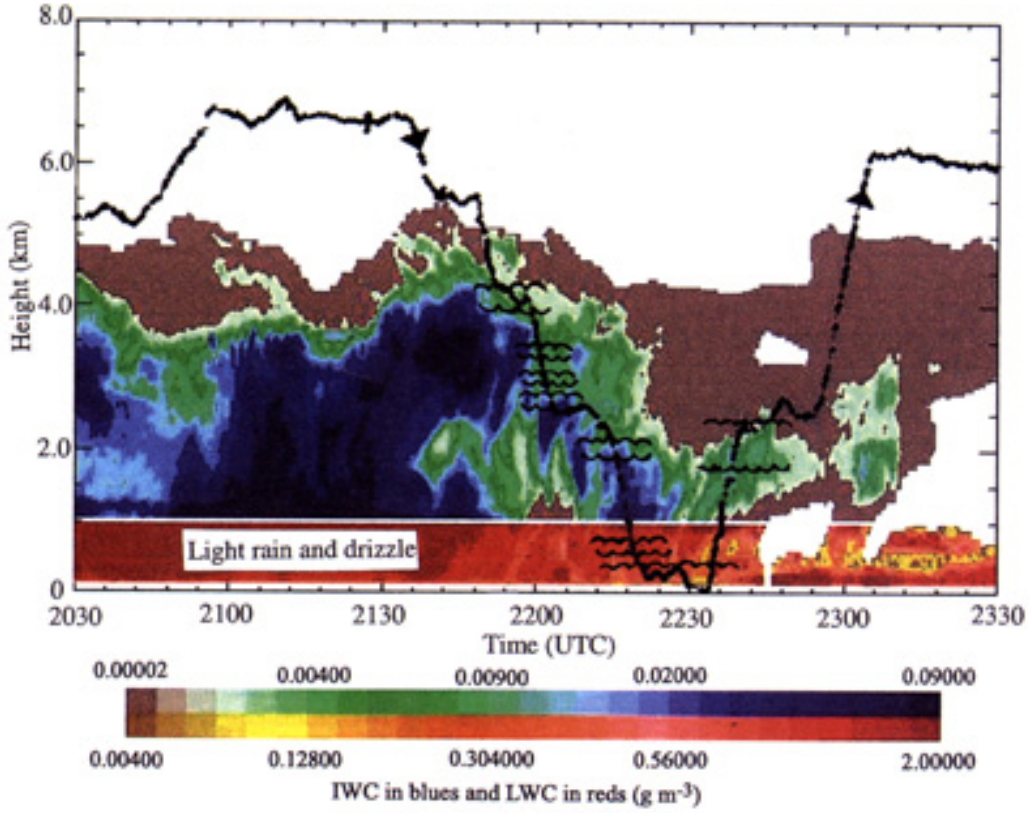

Plate 2. LWC and IWC of mixed-phase, multilayered clouds from 2030 to 2330 UTC, May 29, 1998, derived from the NOAA vertically pointed 35 GHz radar located on the SHEBA ship. The track of the UW Convair-580 aircraft is indicated by the solid thick line with arrows on it. The black scalloping shows the bases and tops of the droplet clouds measured from the aircraft; for example, seven droplet clouds were encountered on the descent of the aircraft.

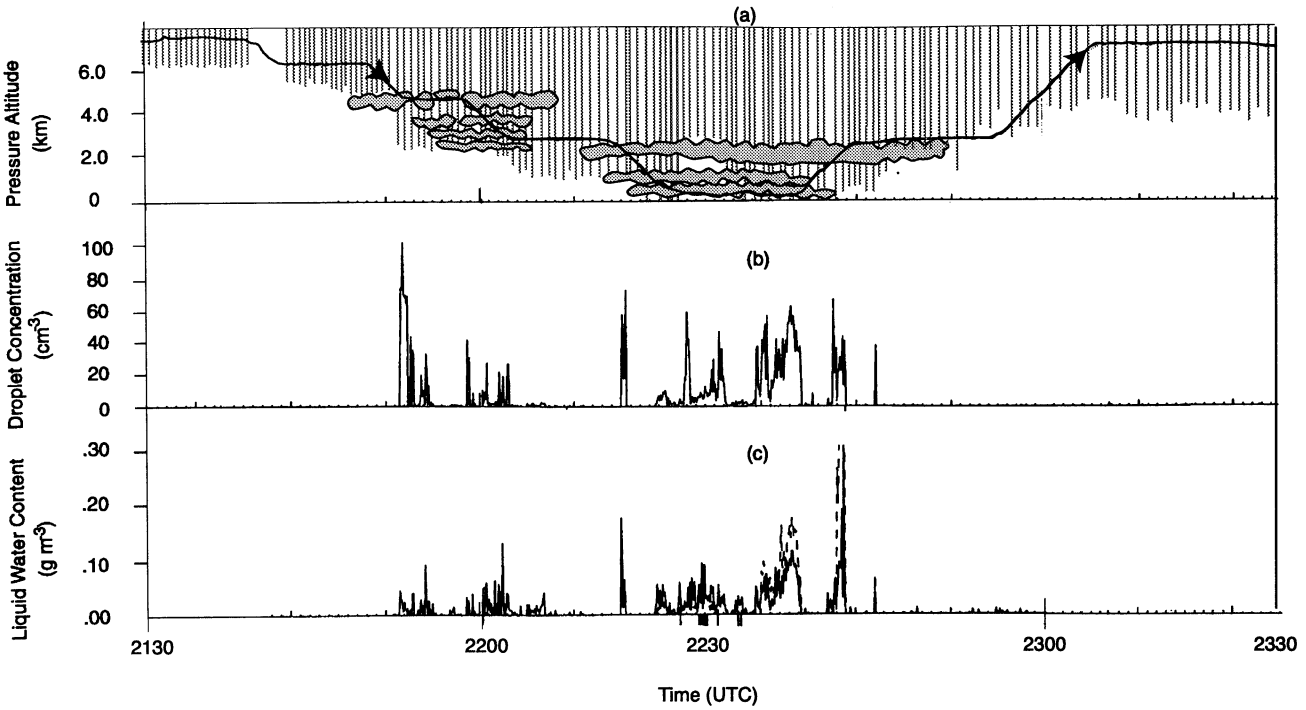

Figure 7. Overview of the clouds sampled by the UW Convair-580 aircraft between 2100 and 2300 UTC on May 29, 1998. (a) Schematic of clouds intercepted. The aircraft track is shown by the thick solid line with arrow on it. The shaded region indicates cloud liquid water, the vertical lines show where only ice was encountered. (b) In situ measurements of droplet concentrations. (c) In situ measurements of liquid water content from the FSSP-100 (solid line) and the PVM-100 (dashed line).

descent and the ascent legs of the Convair flight near and over the ship.

Figure 7a shows a schematic of the clouds intercepted by the UW Convair-580 aircraft on May 29 from just before its descent over the ship to the time it again reached cruising altitude before departure (a time period of about 2 hours). Figure 7 depicts a remarkable degree of cloud complexity. Several types of cloud structures were encountered: all liquid, all ice, and mixed phase. As many as 12 cloud layers were detected over the ship! The details of these many cloud layers are listed in Table 2. Figure 8 shows samples of ice particles imaged in the highest coldest cirriform clouds down to the lowest level that ice was detected (about 800 hPa). This figure shows the growth of ice to just below 700 hPa, followed by diminution in sizes until a few crystals fell into the lowest altocumulus layer where they increased somewhat in size (and also triggered the production of ice splinters) before completely evaporating about 700 m below cloud base.

As expected for this complex system, neither the 35 GHz radar reflectivity display (not shown) nor the retrieved IWC and LWC fields (Plate 2) were able to resolve the many individual cloud layers or to distinguish between cloud and virga. By combining information from more of the remote sensors and using more sophisticated algorithms, it may be possible to obtain more realistic detail from the shipboard measurements, but this remains to be demonstrated. In the remainder of this section, we describe the structures of the clouds and virga that were measured from the aircraft, which illustrate the extreme complexity of the system.

As the aircraft began its descent to the ship from 6.5 km (–36°C), a nearly invisible patch of cirriform clouds was sampled. This patch was probably similar to the highest cirriform clouds that had passed over the ship a few hours earlier. A brief ice-free zone was encountered, followed by a second region of visibly transparent ice crystal cloud at 5.45 km (–28.5°C). The top of these ice crystal clouds corresponded to the general level of the precipitating cloud immediately over the ship. For the most part, these clouds, as seen from a distance, consisted of an altocumulus-like (perlucidus variety) layer that spawned ice crystal fall streaks under small liquid-phase cloudlets. However, only ice crystals were sampled along the descent of the aircraft to the ship.

In both of the two ice crystal clouds, the crystals were largely irregular bullet rosettes, columns, and plates. No riming was seen in the CPI images from these cirriform clouds. The concentrations of ice particles ≥100 μm MD averaged 0.22 per liter with a peak concentration of 0.98 per liter. However, the total concentration of ice particles, including particles down to 5 μm MD, frequently exceeded 100 per liter in some of the nearly transparent "puffs" of these clouds.

The second region of ice crystals mentioned above was more horizontally and vertically extensive; it extended from 5.45 km all the way down to the tops of a mainly liquid altocumulus perlucidus layer at 4.31 km (–20.5°C). The concentrations of ice particles ≥100 μm MD in this lower cirriform cloud were low, averaging 0.23 per liter with a peak concentration of 0.80 per liter. However, many of the ice particles were smaller than 100 μm. Thus the peak concentration of ice crystals estimated by the CPI probe in this lower cirriform cloud was more than 100 per liter in very localized regions, similar to that in the cirriform cloud above.

The altocumulus layer at 4.31 km was as thick as 340 m, with its lowest base at 3.96 km (–17.5°C); it was neither contiguous in the vertical or horizontal. Also present in the

Table 2. Summary of Microstructural Properties of Clouds Over the SHEBA Ship on May 29, 1998, Derived From in Situ Measurements Aboard the UW Convair-580 Research Aircraft

Time of Intercept (hhmm:ss, UTC)	Type of Cloud	Cloud Top Height (km)	Cloud Top Temperature (°C)	Cloud Base Height (km)	Cloud Base Temperature (°C)	Cloud Depth (m)	Average Droplet Concentration (cm^{-3})	Average Liquid Water Content (g m^{-3})	Maximum Liquid Water Content (g m^{-3})	Average Tail of the Droplet Spectrum (μm)	Maximum Tail of the Droplet Spectrum (μm)	Average Effective Radius of Cloud Droplets (μm)	Liquid Water Path (g m^{-2})*	Average Concentration of Drizzle Drops (per liter)	Maximum 1 km Drizzle Drop Concentration (per liter)	Average Ice Particle Concentration (per liter)	Maximum 1 km Ice Particle Concentration (per liter)	Types of Ice Particles
2125:01-2136:05	cirriform	8*	<-37*	—	—	—	0	0	0	0	0		0	0	0	0.22	0.98	solid columns, plates, side planes, irregulars
2142:56-2151:36	cirriform	8*	<-37*	—	—	—	0	0	0	0	0		0	0	0	0.23	0.80	solid columns, plates, side planes, irregulars
2151:36-2158:54	alto-cumulus	4.31	-20.5	3.96	-17.5	340	40	0.03	0.11	15	26	7.8	10	0	0	1.87	8.42	plates, side planes, columns, rimed particles, irregulars
2200:41-2200:49	alto-cumulus	3.45	-13.5	3.35	-13	100	18	0.05	0.09	23	26	12.1	5	0	0	11.00	-	
2202:21-2202:37	alto-cumulus	2.89	-9.2	2.80	-8.8	90	14	0.03	0.09	24	35	13.7	2.7	0	0	6.60	7.07	stellar, plates, dendrites, rimed particles, irregulars
2202:55-2203:08	alto-cumulus	2.76	-8.5	2.66	-7.7	100	21	0.02	0.05	17	24	10.7	2.0	0	0	5.30	5.37	stellars, dendrites, rimed particles, irregulars
2215:02-2215:30	alto-cumulus	2.17	-4.7	2.00	-3.9	170	50	0.09	0.23	21	26	9.1	15	0	0	0.35	0.63	needles, columns, irregulars
2218:49-2219:58	stratus	0.72	-1	0.50	0.1	220	7	0.04	0.06	21	26	13.9	9	0	0	0.00	0.00	none
2211:14-2234:13	stratus	0.34	-1.1	0.12	-0.1	220	27	0.09	0.25	19	26	11.2	20	0.02	0.37	0.00	0.00	none
2235:21-2235:22	stratus	0.83	-0.6	0.82	-0.5	10	9	0.01	0.01	13	14	7.3	0.1	0	0	0.00	0.00	none
2237:22-2242:12	strato-cumulus	2.37	-5.9	1.61	-1.6	760	27	0.09	0.32	21	31	15.3	68	0	0	4.11	15.00	solid columns, plates, needles, sheaths, irregulars, rimed particles
2242:12-2307:15	cirriform	7*	<-33*	2.37	-5.9	>5000	0	0	0	0	0		0	0	0	0.72	6.72	plates, solid columns, bullet rosettes, irregulars

*Estimate.

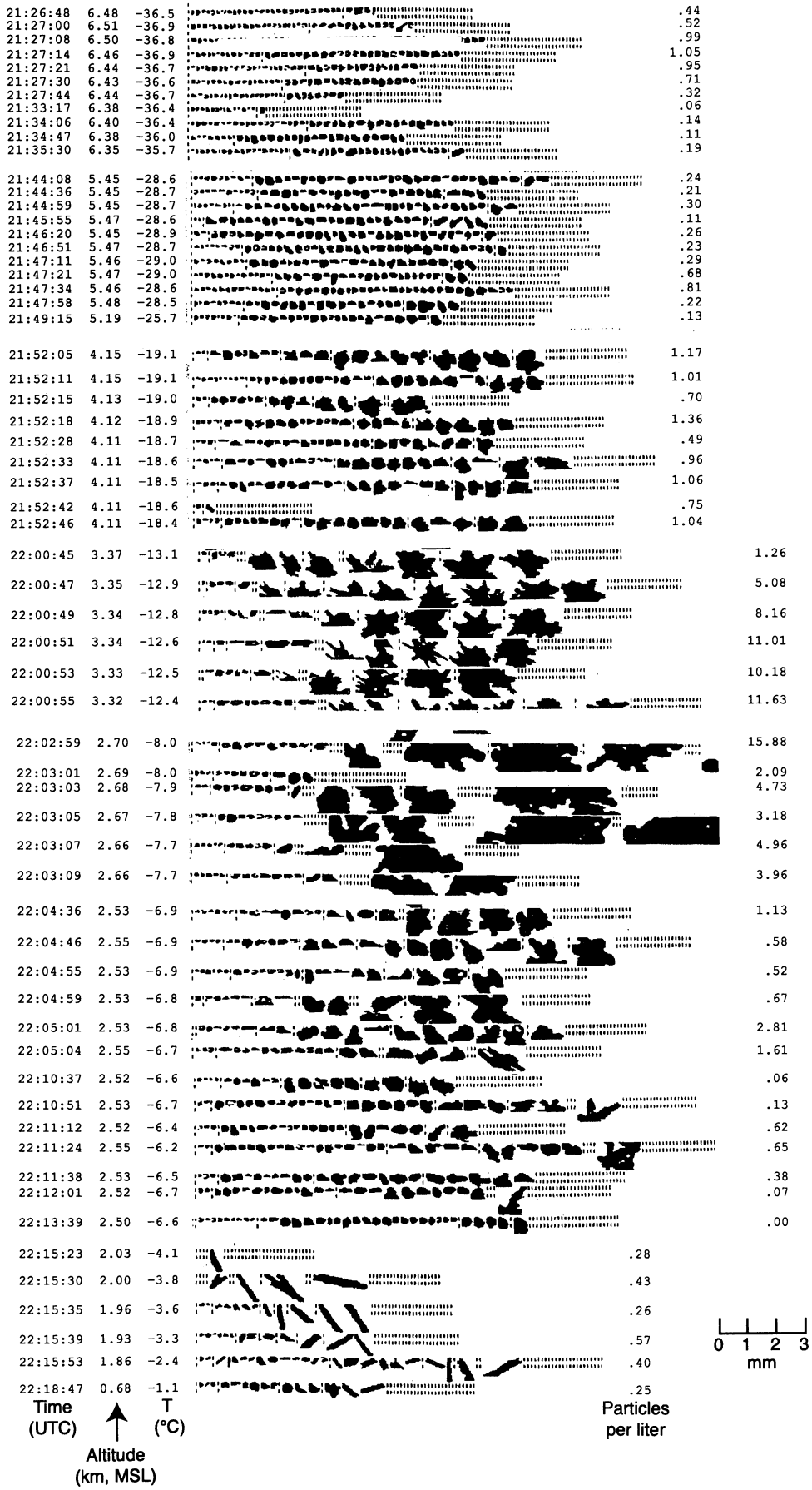

Figure 8. Representative samples of PMS 2-D cloud probe imagery obtained during the descent of the UW Convair-580 aircraft to just above the SHEBA ship on May 29, 1998. The small vertical tick marks denote the beginning and end of size bins 100 μm in width.

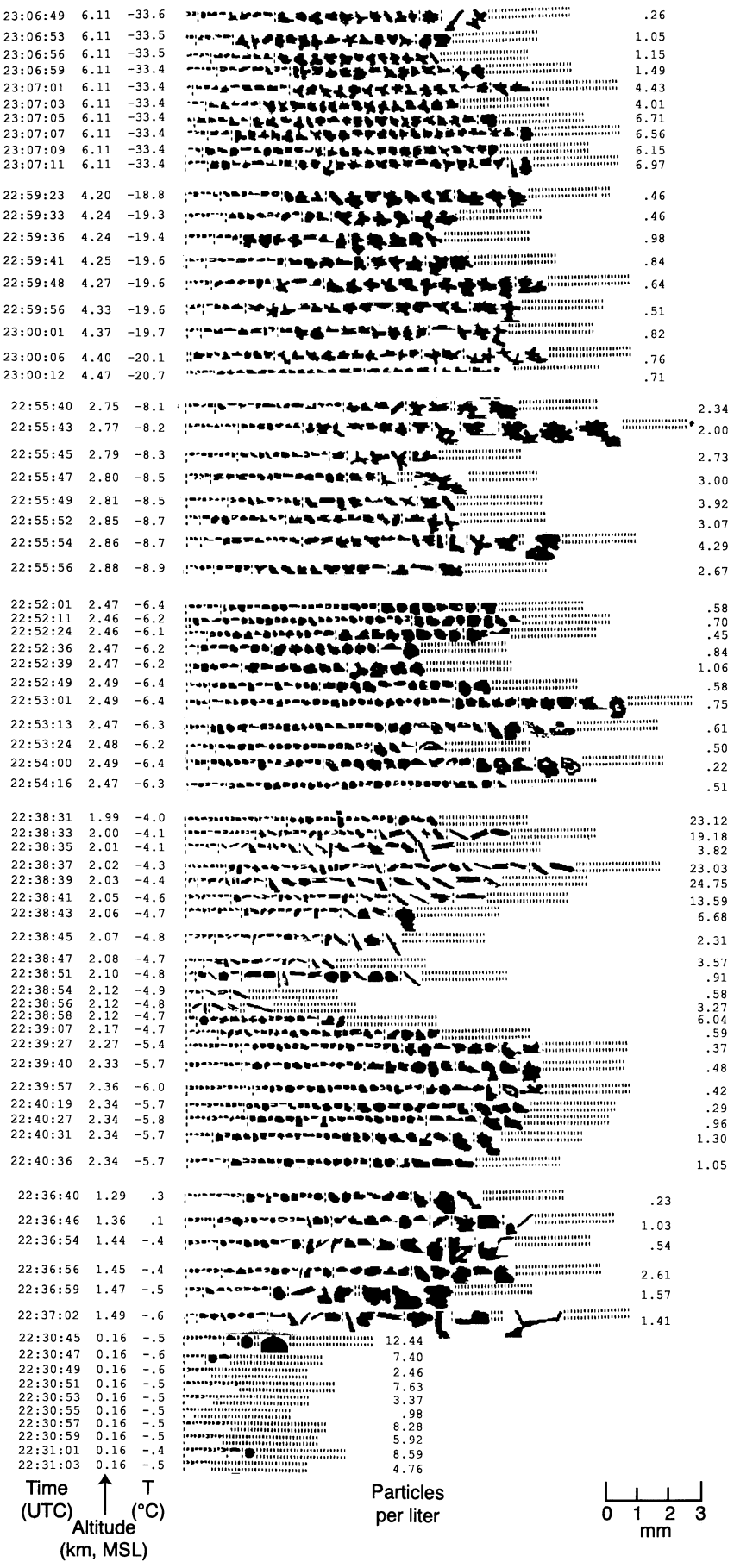

Figure 9. As for Figure 8 but for the ascent of the aircraft.

vicinity of the ship, and spanning several layers of separate, scattered patches of altocumulus clouds (Table 2), were a few isolated convective altocumulus cells (altocumulus floccus or castellanus) with dense, opaque fall streaks. Except for their great height above the ground, some of these resembled "towering cumulus" clouds. A thick plume of ice particles in a fall streak from one of these cells was sampled from the aircraft between 2154 and 2155 UTC. Heavily rimed ice particles approaching graupel-like snow were encountered (Figure 8), which indicates that these ice particles formed in a younger stage of the altocumulus turret when liquid water was significant. The maximum concentration of ice particles ≥100 μm MD in this fall streak was about 10 per liter, about 10 times greater than in adjacent regions. However, the concentrations of much smaller particles indicated by the CPI were very much greater, briefly reaching more than a thousand per liter in several portions of this fall streak. In the altocumulus layer itself, the tail of the droplet spectrum was as large as 26 μm diameter, which reflects the low average droplet concentration (30 cm^{-3}). The maximum LWC was about 0.10 g m^{-3}.

A second thin layer of altocumulus clouds was encountered at 3.45 km (–13°C) with a base at 3.35 km (–12.5°C). The droplet concentration was low (18 cm^{-3}) and the droplet spectra again rather broad with a tail near 26 um diameter. The maximum LWC was 0.09 g m^{-3}. Stellar and dendritic-like ice crystals fell into this altocumulus layer, with light riming on some of the crystals (Figure 8). Ice crystal concentrations increased from several per liter to 10-20 per liter below this altocumulus layer (Table 2), apparently due to new crystal formation.

A third thin layer of altocumulus was intercepted between 2.89 and 2.80 km (–9.2° to –8.8°C). Droplet concentrations were again very low, about 15 cm^{-3}; the maximum LWC was between 0.15 and 0.20 g m^{-3}. The droplet spectrum was very broad with a tail at 35 μm diameter, which indicates drop growth by collisions. A few supercooled drops larger than 50 μm diameter were present. The dendritic crystals falling into this 90 m thick layer increased in size while decreasing in concentration. Light to moderate riming of these crystals was indicated in the PMS 2-D cloud imagery (Figure 8).

Yet another layer of altocumulus clouds was encountered with its top at 2.76 km (–8.5°C) and base at 2.66 km (–7.7°C). The droplet spectra in some regions of this 100 m thick layer were narrower than in the two cloud layers above, with the maximum tail at 24 μm diameter. Once again, droplet concentrations were low (20 cm^{-3}). Ice particles from aloft also fell into this layer, but no enhancement of concentrations was observed.

Below the fourth altocumulus cloud layer, ice particles (virga) were observed, until the crystals evaporated at 2.50 km. The bottom of this evaporation zone was just above the tops of a fifth altocumulus layer, located at 2.17 km. This lowest altocumulus layer was 170 m thick with a base at 2.00 km. Top and base temperatures were –4.7°C and –3.9°C, respectively. The droplet concentration in this last altocumulus layer was 50 cm^{-3}. In spite of the relatively high cloud top temperature the lowest altocumulus layer appeared to spawn independently a few needle and sheath ice crystals in concentrations of about 0.5 per liter. The tail of the droplet spectrum (26 μm), combined with the appropriate temperature range, made this cloud eligible for the production of secondary ice particles by splinter production during riming [*Rangno and Hobbs,* 1990, this issue]. Ice crystals falling from this lowest altocumulus layer were detected to 1.8 km, or about 1 km above the tops of the boundary layer stratus/stratocumulus deck that shrouded the ship in fog and drizzle.

The integrated effect of these many cloud layers, several independently shedding ice particles, was to produce the appearance from below of a deep, gray altostratus sheet with only hints of embedded droplet clouds. The disk of the Sun was not visible. From below the bottom of the virga, it could be seen that in the vicinity, precipitation extended to lower heights than that intercepted by the aircraft. The bottom of the visible virga also marked the approximate height of the freezing level above the boundary layer stratus (Plate 2).

The top of the boundary layer stratus was located at 0.68 km (–1.0°C) at the base of a temperature inversion. The maximum temperature just above cloud top was 1.6°C. Droplet concentrations in the stratus were very low (10-30 cm^{-3}), with a moderately broad spectrum extending to 23-26 μm diameter. Precipitation-sized drops were encountered in this cloud. The concentration of drizzle (≥200 μm diameter) drops reached several per liter in some regions, while the concentrations of embryonic drizzle drops (50-200 μm diameter) were tens per liter.

While sampling the stratus clouds, very light freezing rain (consisting of drops >500 mm diameter) was intercepted (Figure 9). These supercooled raindrops fell from the multilayered altostratus/altocumulus decks described above. A few drops >2 mm diameter were also encountered. However, the maximum concentration of millimeter-sized drops was less than 0.5 per liter in the heaviest portion of the rain.

Following 15 min of sampling in the stratus clouds, the aircraft ascended through the clouds overhead, where a quite different cloudscape was encountered than that in the descent. The lowest level to which ice crystals descended was now lower than earlier, down to 1.29 km or only about 0.5 km above the tops of the stratus clouds. The crystals encountered were almost exclusively needles, sheaths, and their fragments, although some low-temperature-type crystals were also encountered (Figure 9). The total concentrations of ice particles ≥100 μm MD was as high as 30 per liter.

On the ascent from the ship, the lowest of the five altocumulus layers encountered on the descent was now about twice as thick and its base low enough to be termed "stratocumulus." The base was now located at 1.68 km (–2°C) and the top at 2.12 km (–5.9°C). Droplet concentrations were still very low (20-40 cm^{-3}). The greater cloud depth led to a very broad droplet spectrum, with a tail reaching 31 μm diameter. Also, the concentrations of drops >23 μm was greater than 20 cm^{-3} in some regions of this cloud. Isolated drops with diameters >50 μm, formed by collision-coalescence, were also present.

The broader droplet spectrum in this stratocumulus layer, with temperatures between –2° and –6°C, made it ripe for the riming-splintering process [*Hallett and Mossop,* 1974; *Mossop,* 1985]. Consequently, in spite of the slight supercooling of this layer, ice particles in concentrations of 10-30 per liter fell from it.

As the aircraft climbed out of the altocumulus/stratocumulus layer, low concentrations (<0.2 per liter) of low-temperature ice crystals were detected. These could have "triggered" ice particles by riming-splintering in the altocumulus/stratocumulus below. The crystals falling into this layer fell from the same higher cloud layers that were over the boundary

layer stratus during the aircraft descent. However, the clouds aloft now consisted of ice alone; no further liquid water layers (embedded in the altocumulus layers) were encountered. Hence four of the five liquid-mixed phase layers moved away or dissipated in the hour or so between the aircraft sampling times.

The concentrations of ice particles measured in the aircraft ascent ranged from less than 1 per liter to as high as 10 per liter in the climb out from 2.12 km to 6.1 km. The top of the ice crystal cloud was not intercepted, but it was estimated to lie within 1 km of the maximum flight level or at about 7 km. Visibility was nearly unrestricted in this thin ice crystal cloud.

The ice crystals encountered during the ascent consisted largely of unrimed short columns, plates, stellars, stellars with sector-like extensions, and bullet rosettes (Figure 9, top and middle). The concentrations of ice crystals indicated by the CPI, including those down to about 5 μm MD, were generally a few hundred per liter during the ascent.

The tops of clouds, which were spawning precipitation, were well measured by the radar, since precipitation-sized particles were present within 100 m of these tops. However, Plate 2 shows that the many cloud droplet layers encountered by the Convair-580 aircraft were not detected by the 35 GHz radar. This is probably due to the fact that few drops >40 μm diameter were present in the midlevel clouds [*Hobbs et al.*, 1985]. The boundary layer stratus, which contained some drops >50 μm and some drizzle-sized drops (≥200 μm diameter), was detected clearly by the radar, with numerous fall streaks of drizzle apparent (Plate 2, post 2300 UTC).

5. Summary and Conclusions

The descriptions given here of two case studies of clouds over the Arctic Ocean show that clouds in this region can be very complex. The June 3 case described here consisted of a single layer of thin altocumulus cloud, containing liquid water and a few ice particles, with virga beneath the cloud base. In this case, the cloud top height depicted by the 35 GHz radar was close to that measured from the aircraft; although, because of the virga, the radar gave the impression of a lower cloud base than that documented from the aircraft. Also, because of the sensitivity of the 35 GHz radar to ice particles, it was not possible to retrieve reliable cloud liquid water parameters using the radiometer-radar technique. Nevertheless, the shape of the vertical profile of ice particle sizes retrieved from the remote sensing measurements were similar to the in situ measurements from the PMS 2-D cloud probe (see Figure 5b).

In the May 29 case described here, 12 cloud layers connected by virga were present. Within these clouds the following processes were active: collision-coalescence in the boundary layer and middle-layer clouds, ice enhancement in the middle-layer clouds, fragmentation of crystals, condensation freezing and/or contact nucleation of cloud drops, growth of precipitation particles via riming, and probably deposition nucleation of ice in the lowest temperature cirriform clouds. The remote sensing measurements from the ship did not resolve the cloud layers, instead it depicted them as a single deep precipitating system. A perusal of the entire SHEBA 35 GHz cloud-radar imagery indicates that situations with clouds with tops above the 700 hPa level ("deep" arctic clouds) comprise about half of the SHEBA data set. For these cases, in particular, it may not be possible to derive detailed information on cloud properties from remote sensing measurements.

Acknowledgments. The crews of the Convair-580 and the *des Groseillers* are thanked for their help in collecting data. This research was supported by the following grants to the University of Washington: OPP-9808163 from the NSF Arctic Science Section, NAG1-2079 from the NASA Radiation Program, and NASA Cooperative Agreement NCC5-326.

References

Alvarez, R. J., W. L. Eberhard, J. M. Intrieri, S. P. Sandberg, and K. W. Koenig, Cloud backscatter and phase measured in the Arctic using ETL's DABUL lidar, in *4th International Symposium on Tropospheric Profiling*, Am. Meteorol. Soc., Boston, Mass., 1998.

Atlas, D., S. Y. Matrosov, A. J. Heymsfield, M.-D. Chou, and D. B. Wolff, Radar and radiation properties of ice clouds, *J. Appl. Meteorol., 34,* 2329–2345, 1995.

Dye, J. E., and D. Baumgardner, Evaluation of the forward scattering spectrometer probe, part I, Electronic and optical studies, *J. Atmos. Oceanic Technol., 1,* 329–344, 1984.

Frisch, A. S., G. Feingold, C. W. Fairall, T. Uttal, and J. B. Snider, On cloud radar and microwave radiometer measurements of stratus cloud liquid water profiles, *J. Geophys. Res., 103,* 23,195–23,197, 1998.

Gerber, H., B. G. Arends, and A. S. Ackerman, New microphysics sensor for aircraft use, *Atmos. Res., 32,* 235–252, 1994.

Hallett, J., and S. C. Mossop, Production of secondary ice particles during the riming process, *Nature, 249,* 26–28, 1974.

Heymsfield, A. J., and J. L. Parrish, A computational technique for increasing the effective sampling volume of the PMS two-dimensional particle size spectrometer, *J. Appl. Meteorol., 17,* 1566–1572, 1978.

Hobbs, P. V., and A. L. Rangno, Ice particle concentrations in clouds, *J. Atmos. Sci., 36,* 2523–2549, 1985.

Hobbs, P. V., and A. L. Rangno, Microstructures of low and middle-level clouds over the Beaufort Sea, *Q. J. R. Meteorol. Soc., 124,* 2035–2071, 1998.

Hobbs, P. V., N. T. Funk, R. R. Weiss Jr., J. D. Locatelli, and K. R. Biswas, Evaluation of a 35 GHz radar for cloud physics research, *J. Atmos. Oceanic Technol., 2,* 35–48, 1985.

Lawson, R. P., and T. L. Jensen, Improved microphysical observations in mixed phase clouds, Preprints, in *AMS Conference on Cloud Physics,* Am. Meteorol. Soc., Boston, Mass., 1998.

Matrosov, S. Y., Variability of microphysical parameters in high-altitude ice clouds: Results of the remote sensing method, *J. Appl. Meterol., 36,* 633–648, 1997.

Matrosov, S. Y., Retrievals of vertical profiles of the cloud microphysics from radar and IR measurements using tuned regressions between reflectivity and cloud parameters, *J. Geophys. Res., 104,* 16,741–16,753, 1999.

Moran, K. P., B. E. Martner, M. J. Post, R. A. Kropfli, D. C. Welsh, and K. B. Widener, An unattended cloud-profiling radar for use in climate research, *Bull. Am. Meteorol. Soc., 79,* 433–455, 1998.

Mossop, S. C., Secondary ice particle production during rime growth: The effect of drop size distribution and rimer velocity, *Q. J. R. Meteorol. Soc., 111,* 1113–1124, 1985.

Rangno, A. L., and P. V. Hobbs, Ice particle concentrations and precipitation development in small polar maritime cumuliform clouds, *Q. J. R. Meteorol. Soc., 117,* 207–241, 1990.

Rangno, A. L., and P. V. Hobbs, Ice particles in stratiform clouds in the Arctic and possible mechanisms for the production of high ice concentrations, *J. Geophys. Res.,* this issue.

Shupe, M. D., T. Uttal, S. Y. Matrosov, and A. S. Frisch, Cloud water contents and hydrometeor sizes during the FIRE Arctic Clouds Experiment, *J. Geophys. Res.,* this issue.

P. V. Hobbs and A. L. Rangno, Department of Atmospheric Sciences, University of Washington, Box 351640, Seattle, WA 98195-1640. (phobbs@atmos.washington.edu)

M. Shupe, Science and Technology Corporation, Hampton, VA 23666.

T. Uttal, NOAA Environmental Technology Laboratory, Boulder, CO 80303.

(Received December 22, 1999; revised May 10, 2000; accepted May 11, 2000.)